

## THE SURFACE BRIGHTNESS TEST FOR THE EXPANSION OF THE UNIVERSE. I. PROPERTIES OF PETROSIAN METRIC DIAMETERS

ALLAN SANDAGE

The Observatories of the Carnegie Institution of Washington, The Johns Hopkins University, and Space Telescope Science Institute

AND

JEAN-MARC PERELMUTER

The Johns Hopkins University and Space Telescope Science Institute

*Received 1989 May 15; accepted 1989 August 18*

### ABSTRACT

In this first paper of a series, we begin a study of the surface brightness (SB) properties of E and S0 galaxies over a range of absolute magnitudes. The purpose is to determine the intrinsic variation of the SB at given  $M_{B_T}$  values. This is to lay a foundation for a practical observational test of the Tolman prediction that the bolometric SB decreases as  $(1+z)^4$  in an expanding universe and  $1+z$  if the redshift is not caused by expansion. The test has not yet been done satisfactorily due to (1) lack of knowledge of the intrinsic scatter of  $\langle SB \rangle$  at a given  $M_{B_T}$  in any sample of galaxies at a given  $z$ , and therefore no notice has been taken to date of the size of the sample needed to obtain an answer, and (2) lack of use of a practical operational definition of a metric (rather than an isophotal) angular diameter over which to measure an average SB for any galaxy.

The definition of the Petrosian  $\eta$  diameter is set out as a practical operational procedure. Properties of the  $\eta(r)$  function are illustrated for the Hubble, Oemler, de Vaucouleurs, and King SB fitting templates for E galaxies, and also for the real galaxies of NGC 1272, NGC 3379, NGC 4267, and NGC 4697 using measured photometric data from the literature. Properties of the resulting  $r(\eta)$  metric radii relative to the effective (i.e., half-light) radius,  $r_e$ , are shown for the Oemler and de Vaucouleurs fitting functions. Metric radii far out into the galaxy's image (relative to  $r_e$ ) are still well defined and can be measured in practical applications. It is shown that metric radii, and therefore an average SB inside that radius, can be measured to very large redshifts. Brightest cluster galaxies similar to those in the Virgo cluster are expected to have diameters of  $\sim 6''$  for an  $\eta$  value of 2 mag arcsec $^{-2}$  at a redshift of  $z \simeq 0.7$ . Galaxies  $\sim 4$  mag fainter in the same cluster will still have diameters of  $\sim 1''$ , and therefore should be accessible from the ground, taking into account seeing corrections. The expected apparent magnitudes in the  $R$  bandpass for the brightest cluster galaxies are calculated to be at  $R \simeq 20$  mag for  $z \simeq 0.7$ , averaged over the  $r(\eta = 2$  mag) radius, and  $R \simeq 22$  mag at the  $r(\eta = 2$  mag) Petrosian radius. For galaxies 4 mag into the luminosity function in such clusters, these flux levels are  $R = 24$  mag inside the  $r(\eta = 2$  mag) radius, and  $R = 26$  mag at that radius. These angular diameter and flux values are well within ground-based capabilities with existing telescopes, detectors, and active optic wavefront correctors. This makes the Tolman SB test for the expansion of the universe possible in practice now if problems concerning particular evolutionary corrections can be understood.

*Subject headings:* cosmology — galaxies: photometry

### 1. INTRODUCTION

Despite the evident success of the standard model of cosmology in explaining so much, and despite the "lack of a reasonable alternative physical basis for the redshift" (Geller and Peebles 1972), there is no direct proof yet that the universe actually expands. The only known fundamental test that the redshift is caused by a secular change in the scale factor of the metric is that proposed by Tolman (1930, 1934) and discussed in detail by Hubble and Tolman (1935). In the presence of expansion, the bolometric surface brightness (hereafter SB) of a "standard source" should vary as  $(1+z)^{-4}$ . In the absence of expansion, where there is nevertheless a redshift due to an unknown cause, the SB should vary as  $(1+z)^{-1}$ .

The test, so simple in principle, has not been carried out in any convincing manner to date because of difficult technical problems, although several discussions of segments of the test have been made.

Geller and Peebles (1972) discuss the change of diameter ( $\theta$ ) of first-ranked galaxies with redshift ( $z$ ) and the change of apparent magnitude,  $m$ , within that diameter as  $z$  increases.

The ratio of the apparent luminosity,  $l$ , to  $\theta^2$  is the SB. Although  $\theta$  and  $l$  each depend in some manner on the spatial geometry through the deceleration parameter  $q_0$  (Sandage 1961a), the dependence cancels exactly in the  $l/\theta^2$  ratio, making the SB independent of  $q_0$ . Surface brightness, as such, was not available for the galaxies whose diameters were discussed by Geller and Peebles; hence, they discussed the  $\theta(z)$  and  $m(z)$  relations separately.

Djorgovski and Spinrad (1981, hereafter DS) have also concentrated on a measured metric angular diameter; that is, one related to linear measure rather than the isophotal properties of the image, defined in an elegant way (see below) by Petrosian (1976). They attempted to find either  $q_0$  by comparing observations with the theoretical  $\theta(q_0, z)$  family of curves derived from the standard model, and/or to find the evolution of  $\theta$  with  $z$  using an assumed value of  $q_0$ ; the evolutionary claim (based on the residuals of the observations from the theory) then being model dependent. DS did not discuss the SB test itself, having shown that no reasonable standard model without evolution can fit their  $r(z)$  observational data (DS, Fig.

5) for the first few ranked galaxies in a number of clusters. They concluded that evolution of their Petrosian metric diameter has occurred with  $z$  for galaxies in their sample.

Three types of evolution can be expected. The simplest is the change in total galaxy luminosity caused by evolution of the individual member stars. Such evolution will affect neither the "effective" (see below) nor the Petrosian metric diameters unless the luminosity change depends on radius. Petrosian diameters are those where the ratio of two surface brightness values in a given galaxy has a particular (fixed by decision) value. Clearly, a radius-independent luminosity evolution will cancel in this ratio, leaving the Petrosian radius unaffected. Of course, the SB value itself, averaged over any given Petrosian radius, will change directly with the evolutionary effect and must be accounted for, as we will discuss later. More serious is dynamical evolution due to cannibalism that may exist in the first few dominant galaxies in rich clusters. These mergers of small galaxies with the largest will, in general, change the size of the original galaxy and hence its Petrosian radii values. Djorgovski and Spinrad interpreted the failure of their data to support the standard model without evolution to this cause.

In lieu of convincing ways to correct for the effect in making the Tolman test, we propose to use the SB properties of many galaxies in a given cluster, not simply the first few ranked where the effect occurs. By sampling over the first several magnitudes of the luminosity function in each cluster, we suppose that cannibalism can be ignored in all but the brightest galaxies. However, to use such data in the comparison of SB values for cluster galaxies at different redshifts requires knowledge of how SB varies systematically with galaxian absolute magnitude. It is this problem that is the subject of this series of papers.

The third evolutionary effect concerns tidal stripping, which, like the second, is also environmental, indigenous to rich clusters. Where it occurs, it affects the outermost parts of the galaxy profile. The inner parts are less vulnerable, causing less effect at smaller radii, thus providing a test and a method of correction. Also, the extent of tidal stripping, like cannibalism, depends on cluster richness, providing a second method of correction via correlations with richness.

Although these three evolutionary problems give warnings that the Tolman test is not without difficulties, we shall, in this series of papers, explore the problem using nearby galaxies where the evolutionary effects are either absent, or where the redshift range is small enough that the data refer to the same epoch. The purpose of these papers is, then, to begin a study of those properties of the Petrosian parameters which we shall need both locally and at large redshifts, and in the absolute magnitude range which we expect to explore. Our aim is to provide a base of calibrations using nearby galaxies upon which the evolutionary problems can later be added.

Galaxies do not have well-defined edges; their luminosities decrease continuously outward, showing no discernible edge until very faint surface brightnesses are reached—so faint as to make it difficult to accurately measure such an edge. The *apparent* edge of an image as it appears to the eye on hard copy pictures (say, on photographic plates or on CCD reconstructions) occurs at a particular *isophote*, usually where the SB of the galaxy is  $\sim 0.6$  mag fainter than the SB of the night sky (see Humason, Mayall, and Sandage 1956; Appendix A). But *isophotal* diameters are different from *metric* diameters, and their use in performing the Tolman SB cosmological test leads to a much degraded experiment because of the nature of

the ratio of isophotal to metric measure (Sandage 1972, § III). It turns out to be crucial to know what kind of diameter has been measured before discussing the Tolman test. Furthermore, the method used must be crystal clear and simon-pure. For example, there is still a question whether the diameters discussed by Geller and Peebles (1972) were a metric or an isophotal measure. They used data by Baum (1972), which he obtained with a mechanical "galaxy image simulator" in the telescope focal plane.

The operational problem for the observer has always been how to define a metric diameter than can be reasonably used in practice. The suggestion by Hubble and Tolman was to measure the parameter  $a$  in Hubble's (1930) fitting equation

$$B(r) = \frac{B(0)}{(1 + r/a)^2}, \quad (1)$$

used by him to describe the surface brightness profiles of E galaxies. [Here  $B(r)$  is the surface brightness, in units of, say, magnitudes per square arcsecond at radius  $r$ .] Although  $a$  is a metric radius, its determination is impossibly difficult for distance galaxies, because the surface brightness measurements must be made so close to the center of a galaxy before a significant departure from a power-law profile of  $r^{-2}$  occurs. For example, the value of  $a$  for the giant E galaxies NGC 4486 and NGC 4472 in the Virgo Cluster is only  $\sim 10''$ . Therefore, even at the small redshift of  $z = 0.1$ , the value of  $a$  is  $\sim 0.3$  well below the seeing disk. This redshift is too small to provide enough sensitivity for the Tolman SB test, because the cosmic scatter in  $\langle SB \rangle$  at any given absolute magnitude is large compared with the Tolman effect at such small redshifts for real galaxies (see Binggeli, Sandage, and Tarenghi 1984, Fig. 8; and Papers II and III of this series to follow). A much larger redshift range than only to  $z \sim 0.1$  must be used for the test. This requires defining some type of a metric diameter far out in the galaxy profile so that galaxies at large redshift can be used with real observations at the telescope with a practical means of correcting for the seeing profile, whose size should not be larger than that part of the true profile we wish to recover.

Fortunately, the definition of a practical metric diameter is possible because it is known that equation (1), which becomes an  $r^{-2}$  power law at large  $r$ , fails when  $r/a \gtrsim 20$ , making any scale information in the real profile more accurate than for the Hubble template profile. The profiles of real galaxies decrease more steeply than equation (1) at large radii, well modeled by Oemler's (1976) modification of Hubble's law, where a cutoff at large  $r$  is introduced by

$$B(r) = B(0)e^{-(r/\alpha)^2} \left(1 + \frac{r}{\beta}\right)^{-2}, \quad (2)$$

where  $\alpha$  and  $\beta$  are fitting parameters. The strength of the cutoff is measured by the  $\alpha/\beta$  ratio. For the Hubble law in equation (1), this ratio is  $\infty$ . A family of Oemler profiles is generated by varying the  $\alpha/\beta$  ratio and is made unit free by using  $r/\beta$  as the radius measure and by adopting various  $\alpha/\beta$  ratios as the family parameter. Properties of the Oemler profile family are discussed in the next section.

The King (1966) models provide a similar family of profiles that are also progressively cut off at large radii. The parameters similar to the  $\alpha/\beta$  Oemler ratios are the King  $r_t$  and  $r_c$  "tidal radius" and "core radius" specified by the models. The King family is generated by changing the  $r_t/r_c$  ratio.

The de Vaucouleurs (1958) fitting law of

$$\log B(r)/B(r_e) = -3.33[(r/r_e)^{1/4} - 1], \quad (3)$$

is similar to equation (1) for intermediate values of  $r/a$  but has the desired (but quite specific, i.e., there is no *family* of curves) steepening at large radii (see King 1978, Fig. 1). Here  $r_e$  is the radius within which half the total light is contained. We emphasize, however, that  $r_e$  is only a fitting parameter in equation (3). It defines the "half-light radius" only if equation (3) fits exactly any galaxy in question.

Even if equation (3) is not used in any particular galaxy fit, or if it does not satisfy the data for any particular galaxy, another definition of "effective radius,"  $r_e$ , can nevertheless be used operationally with no appeal to any fitting law. In 1962, de Vaucouleurs proposed that the *measured* half-light radius be used to define such a radius. It is clearly a metric rather than an isophotal measure. In practice, the operational definition requires finding the total magnitude of a galaxy by determining the horizontal asymptotic level of the growth curve of magnitude versus radius and interpolating in that curve for the radius of a circular aperture at which the magnitude is 0.75 mag fainter than the asymptote. No appeal to any fitting model is needed. However, very accurate measured magnitude values along the growth curve are required, together with an accurate total magnitude.

## II. THE PETROSIAN METRIC RADIUS DEFINED BY HIS $\eta$ PARAMETER

### a) The $\eta$ Parameter Defined

As mentioned, the half-light effective radius is difficult to measure in practice. A slight error in the intensity level of the horizontal asymptote to the growth curve makes an appreciable error in  $r_e$ . A different definition of a metric radius is desired which does not depend on knowledge of the position of this asymptotic limit.

Petrosian defined such a metric radius using surface brightness ratios in a given galaxy. Such a metric measure, hereafter called the  $\eta$  function radius,  $r(\eta)$ , is the radius where the ratio of the average surface brightness within that radius to the SB at that radius has a particular value  $\eta$ . The  $\eta$  value can, if desired, be expressed in magnitudes. For example, if we wish to set the level of the  $\eta$  ratio at say  $2.5 \log \eta = 2 \text{ mag } s^{-2}$ , we would determine, from the observed intensity profile, at what radius in a given galaxy the average SB within  $r$  [found by integrating the  $B(r)$  profile] is 2 mag brighter than the  $B(r)$  value at that radius.

Petrosian showed that this definition of the  $\eta$  intensity ratio, expressed in magnitudes, is equivalent to

$$\eta(\text{mag}) = 2.5 \log \frac{2d \log r}{d \log L(r)}, \quad (4)$$

which obviously can be expressed in terms of the slope,  $d \Delta \text{ mag} / d \log r$  of the growth curve as

$$\eta(\text{mag}) = 2.5 \log \frac{5d \log r}{d \Delta \text{ mag}}. \quad (5)$$

Equation (4) can be derived as follows.

In terms of intensity ratios,  $\eta(\text{intensity})$  is defined, as above, to be the ratio of the average SB inside  $r_i$  to the SB at  $r_i$ , i.e.,

$$\eta(\text{intensity}) = \frac{\langle B(r_i) \rangle}{B(r_i)}. \quad (6)$$

Hence, by definition

$$\langle B(r_\eta) \rangle = \frac{\int_0^{r_\eta} 2\pi r B(r) dr}{\pi r_\eta^2}. \quad (7)$$

The flux within radius  $r_\eta$  is

$$L(r_\eta) = \int_0^{r_\eta} 2\pi r B(r) dr. \quad (8)$$

Hence,

$$\eta(\text{intensity}) = \frac{L(r_\eta)}{\pi r_\eta^2 B(r_\eta)}, \quad (9)$$

found from the defining equation (6) using equations (7) and (8). Since

$$B(r_\eta) = \frac{dL(r_\eta)}{2\pi r dr} \quad (10)$$

(from eq. [8]), when put into equation (9), gives

$$\eta(\text{intensity}) = \frac{L(r)}{dL(r)} d(\ln r^2), \quad (11)$$

which is equivalent to

$$\eta(\text{intensity}) = \frac{2d \log r}{d \log L(r)}. \quad (12)$$

This is equation (4) as was to be shown, expressed in intensity ratios.

In this and in the next two papers to follow, we have calculated  $\eta$  (intensity) from equation (6) using observed data for particular program galaxies. To do so, we have used equation (7) to find  $\langle B(r_\eta) \rangle$  by numerical integration directly from the  $B(r_i)$  data points, and then equation (6) with the individual  $B(r_i)$  values to find  $\eta(r_i)$ .

Because  $\eta$  is a *ratio* of surface brightnesses in a *given galaxy*, the run of  $\eta$  with  $r$  in that galaxy is immune to many types of systematic effects. For example,  $\eta(r)$  will be wavelength independent if there is no color gradient across the galaxy image. The values of  $\eta(r)$ , where  $r$  is in linear measure such as parsecs, will also be independent of redshift because of such a wavelength independence. Said differently, a "standard galaxy" taken to different distances (redshifts), even if observed in a fixed wavelength band in the observer's frame (that is, even if the detector response is not shifted nor stretched in bandwidth with redshift so as to match the rest wavelength detector response), will have identical  $\eta(r_{pc})$  values as the "standard galaxy" at zero redshift. The value of  $\eta(r)$ , being a ratio, is also independent of absorption, and, as mentioned in § I, of luminosity evolution, provided that the evolutionary change of the SB with time is independent of radius. The  $\eta$  measure of the metric radius is therefore very powerful for all these reasons.

The surface brightness itself, averaged over the radius out to a given  $\eta$  value (which is the parameter we seek), is, of course, not evolution free, nor is it independent of redshift (due to the usual  $K$  correction: Humason, Mayall, and Sandage 1956, Appendix B; Oke and Sandage 1968). The power of the Petrosian  $\eta$  radius is that it is invariant to the many effects that affect  $B(r)$  and hence  $\langle B(r) \rangle$ . Therefore  $\langle B(r) \rangle$ , which is the average over the well-defined  $r(\eta)$  radius, is, itself, well defined, and therefore, well-defined corrections can be made to  $\langle B(r) \rangle$  owing to redshift (i.e., the  $K$  term) and evolution when the

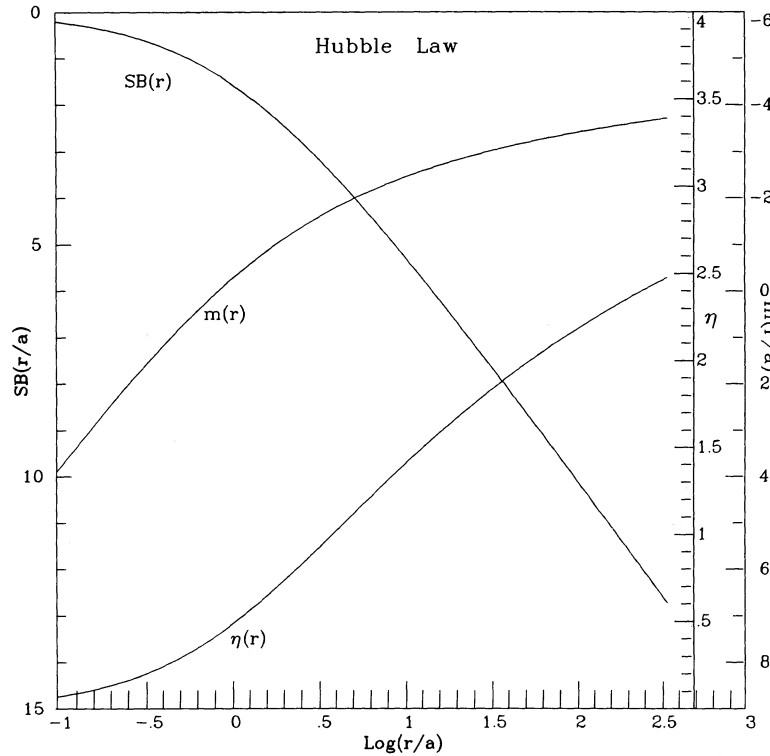


FIG. 1.—Three properties of the Hubble fitting equation are shown as functions of the dimensionless  $r/a$  radius. The surface brightness profile,  $B(r)$ , expressed in magnitudes per unit area, is normalized to  $B(0) = 0$  mag at  $r = 0$ . Scale is along the left ordinate. Scale of the growth curve,  $m(r)$ , is along the outer right ordinate. Scale for the  $\eta(r)$  function is along the inner right ordinate. There is no vertical asymptote to  $\eta(r)$  for the Hubble law because the  $m(r)$  growth curve continues to rise for all  $r$ , giving a total luminosity that has no bound.

Tolman SB test is made using data on “standard” galaxies at high redshift.

#### b) $\eta(r)$ Curves Calculated from the Four Template Fitting Functions

To gain some insight into the properties of the  $\eta(r)$  function for different galaxian intensity profiles, we show in this section families of  $\eta(r)$  curves for the fitting functions of equations (1)–(3), and for the King family of profiles.

Figure 1 shows the  $B(r)$ ,  $m(r) = -2.5 \log L(r)$ , and  $\eta(r, \text{mag})$  curves for the Hubble profile of equation (1). The  $m(r)$  growth curve is calculated from equation (8) using  $B(r)$  from equation (1) as a function of the dimensionless parameter  $r/a$ . The  $\eta(\text{mag}, r)$  curve is calculated from equation (6) using equation (7) to obtain  $\langle B(r_\eta) \rangle$  by numerical integration, and defining  $\eta(\text{mag})$  to be

$$\eta(\text{mag}) = 2.5 \log \eta(\text{intensity}). \quad (13)$$

The templates of the log of the surface brightness  $B(r)$ , the growth curve  $m(r)$ , and the  $\eta(r)$  curves for the Hubble profile are plotted together in the diagram. The scale on the left ordinate is for the  $B(r)$  surface brightness profile, expressed in magnitudes. The two scales along the right ordinate are the growth curve and the  $\eta(r)$  curve, both expressed in magnitudes.

There is no cutoff faster than  $r^{-2}$  in the Hubble profile at large radii; hence, the total intensity for the Hubble profile is infinite. The behavior of  $B(r)$  at large  $r$  as  $(r/a)^{-2}$  in equations (6) and (7) shows that  $\eta(r) = 2 \ln r$  for  $r/a \rightarrow \infty$ . This finite slope of  $\eta(r)$  for all  $r$ , rather than becoming upward unbounded (see Fig. 3), is visible in Figure 1. Note from the definition that  $\eta(r) = 0$  mag at  $r/a = 0$ .

Figure 2 shows a comparison of the  $B(r)$  surface brightness profiles for the Oemler, Hubble (which is an Oemler profile with  $\alpha/\beta = \infty$ ), de Vaucouleurs, and King profiles. The corresponding  $\eta(\text{mag}, r)$  function are compared in Figure 3. Note that all  $\eta(r)$  functions become vertical at the radius where the total luminosity is reached, i.e., where the growth curve becomes asymptotically level. This vertical slope to  $\eta(r)$  at radius where the  $m(r)$  curve growth curve has a horizontal asymptote follows from equation (5) by noting that the growth curve slope,  $d\Delta \text{ mag}/d \log r$ , is zero when the total magnitude is reached.

#### c) Examples of $\eta(r)$ for Real Galaxies

##### i) Practical Problems of the Calculation

We assume here that a table of  $B(r_i)$  surface brightness values is available, listed at various observed radii  $r_i$  along the major axis for any given galaxy. The tabulation seldom begins at  $r_i = 0$ , but at some finite radius, typically at  $r \gtrsim 3''$ .

To begin the numerical integration of equation (6), we need data for the profile to  $r = 0$  that are not supplied by the observations. To obtain an estimate of the interior profile, we have fitted one of the template curves of Figures 2a or 2b to the observations at large radii. This gives an analytical expression of  $B(r_i)$  for small  $r_i$  from the appropriate equation in the set of equations (1)–(3), or from the King (1966) family.

As the numerical integration proceeds outward, the actual data points are eventually reached, which are then used thereafter to provide the  $B(r_i)$  values at the listed  $r_i$  and  $\Delta r_{ij}$  interval values. Often, if the fit of the analytical template is not perfect at the first data point, an artificial spike occurs in the calcu-

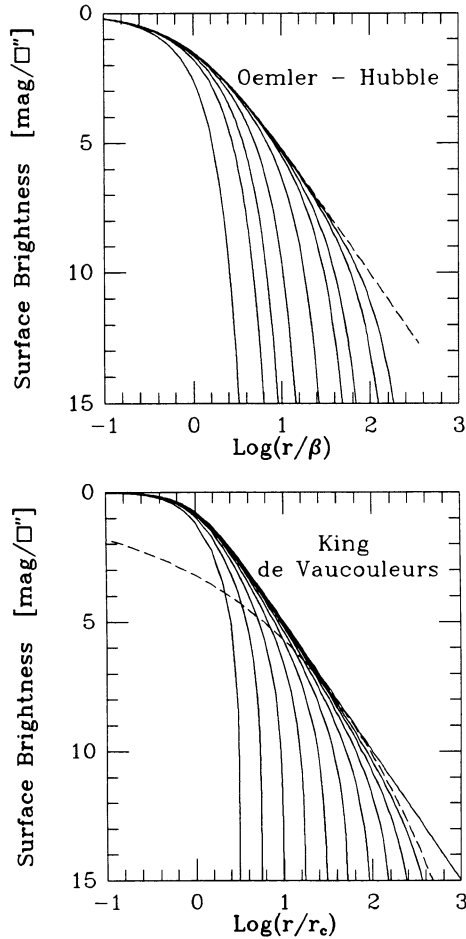


FIG. 2.—(top) Surface brightness profile for the family of Oemler functions with  $\alpha/\beta$  values of 100, 60, 30, 20, 10, 5, 3, 2, and 1, respectively, from right to left. Dashed Hubble profile is the limiting Oemler profile for  $\alpha/\beta = \infty$ . (bottom) Same for the family of King profiles for various  $r_i/r_c$  values. The de Vaucouleurs  $r^{1/4}$  profile is shown as dashed.

lated  $\eta(r)$  at this point. Furthermore, the fit of the template to the outer data points is usually ambiguous enough to permit an appreciable range in the extrapolated central surface brightness,  $B(0)$ . This causes differences in the  $\eta(r)$  values at a given  $r$  for small  $r$ . For this reason, the various  $\eta(r)$  curves that result from the different inward extrapolations to  $B(0)$  differ in their  $r(\eta)$  radii for  $\eta \lesssim 1.3$  mag. However, this difference generally becomes negligible for  $\eta > 1.3$  mag, as we shown in the next paper (Sandage and Perelmuter 1990, hereafter SP). In what follows, it should be kept in mind that the  $r(\eta)$  for  $\eta = 1.0$  mag and  $\eta = 1.3$  mag have larger errors than for  $\eta > 1.3$  mag, when the actual data for galaxies are discussed, owing to this uncertainty in the adopted  $B(0)$  central surface brightness.<sup>1</sup>

<sup>1</sup> We should also note in passing that an artifact of the calculation appears in using eq. (7) as a sum over discrete  $\Delta r$  intervals when  $\Delta r/r > 1$ , such as invariably occurs with real data close to the center. An upturn away from  $\eta(r=0) = 0$  as  $r$  approaches zero is artificial owing to this effect. The problem is overcome when using values from the analytical fits by adjusting the  $\Delta r$  values such that  $\Delta r/r$  is always small, but the problem cannot be avoided using real data for smaller  $r$  where the  $\Delta r_i$  intervals are fixed by the circumstances of the observations. This artificial computational artifact has negligible effect on  $r(\eta)$  for  $\eta > 1$ , which is always the case in practice.

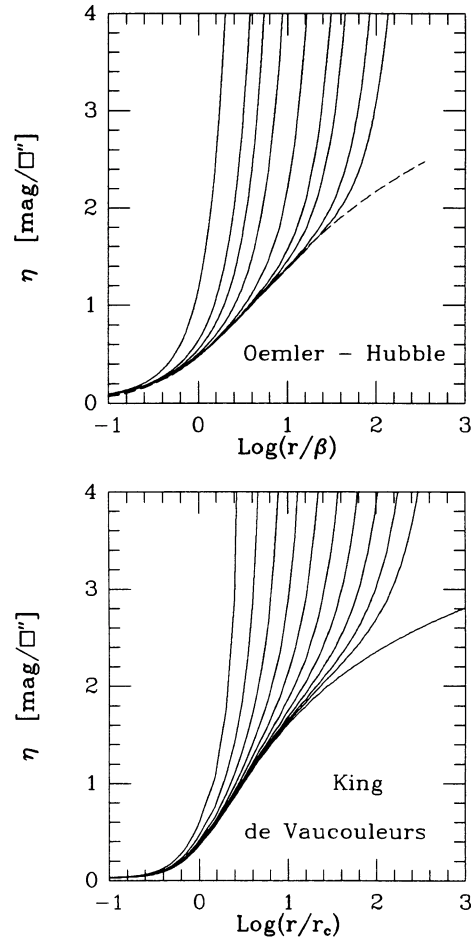


FIG. 3.—The  $\eta(r)$  functions (in  $\text{mag arcsec}^{-2}$ ) for the same  $B(r)$  profiles as in Fig. 2.

#### ii) Wavelength Independence of $\eta(r)$

Wavelength independence of  $\eta(r)$  can be demonstrated by showing the  $\eta(r)$  calculations using data obtained for a given galaxy in different wavelength bands. Figure 4 gives the result using equations (6) and (7) for NGC 4697, where the  $B(r)$  intensity profile has been measured in  $B$  and  $R$  photometric bands by a number of observers, shown in the code to the diagram. The data are from King (1978), Jedrzejewski (1987), Djorgovski (1985), and Jedrzejewski, Davies, and Illingworth (1988, labeled "Illingworth" in Fig. 4). The lack of systematic difference with color between the curves is evident.

The scatter in  $\eta(r)$  between observers shown in Figure 4 is typical of the data we shall be discussing in the papers of this series. Our experience in comparing the  $\eta(r)$  curves for galaxies where several independent  $B(r_i)$  data sets exist by different observers, is that the range of  $\Delta \log r$  at given  $\eta$  values is  $\sim 0.1$ , which is  $\sim 25\%$  range in  $r(\eta)$ . Values as large as  $\Delta \log r \sim 0.3$  do occur, but these are rare. As we show in the next subsection, the run of  $\eta(r)$  is extremely sensitive to small fluctuations in  $B(r_i)$ , either due to errors or to real variations, occasionally causing large uncertainties in  $r(\eta)$  over the range in  $\log r$  values where  $B(r_i)$  is noisy or is ill behaved. Such behavior is due, for example, to (1) extended envelopes, (2) companions, or (3) internal structure, such as a bar. Examples of such behavior are shown in Figures 6 and 7 below.

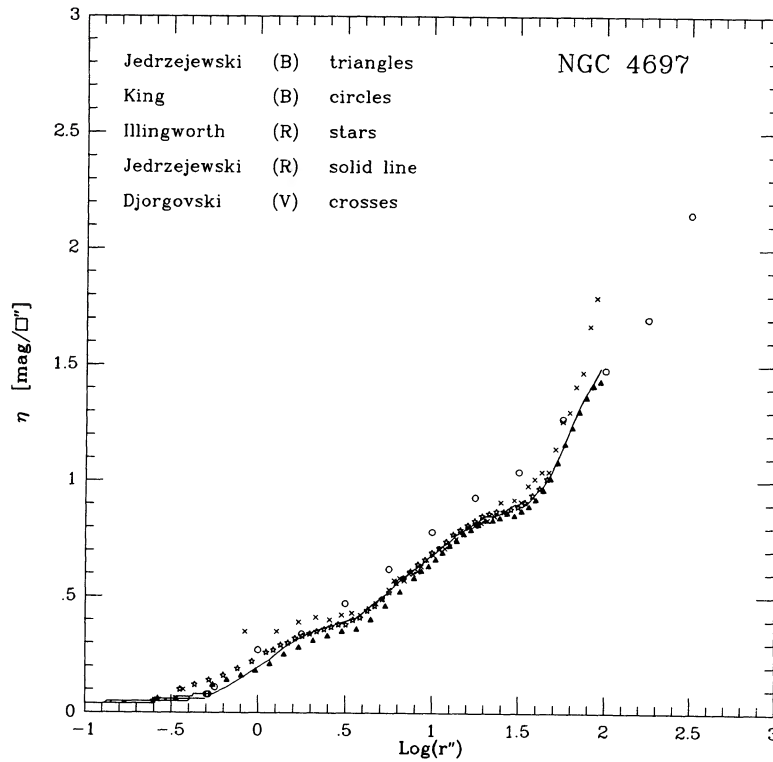


FIG. 4.—Comparison of calculated  $\eta(r)$  curves for NGC 4697 using data from five independent observational programs and three different bandpasses (B, V, and R).

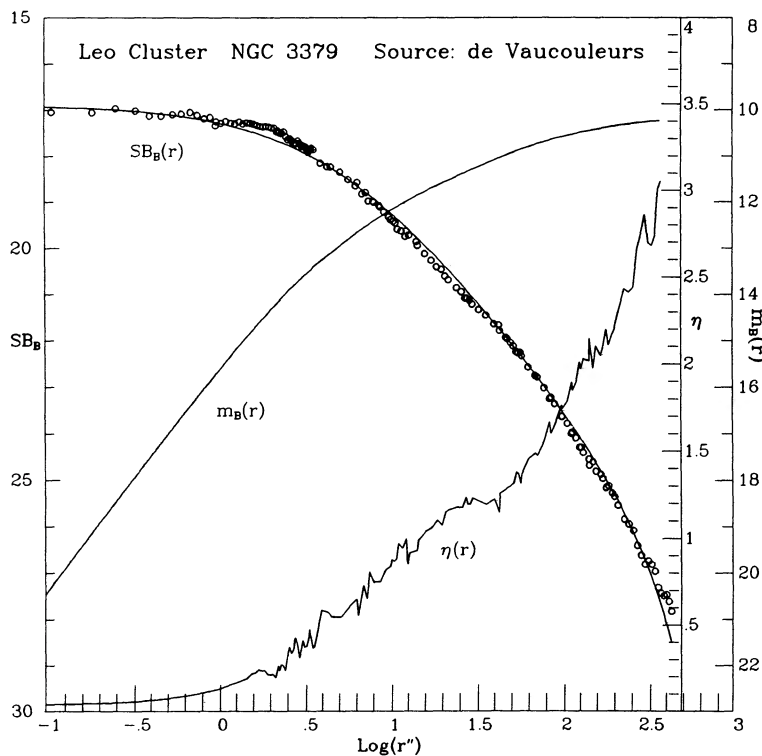


FIG. 5.— $B(r)$ ,  $m(r)$ , and  $\eta(r)$  functions from the observed data for the E0 galaxy NGC 3379 discussed by de Vaucouleurs and Capaccioli (1979). Solid line for the  $B(r)$  profile is an Oemler function with  $\alpha/\beta = 70$ .

iii) Examples of Individual  $\eta(r)$  Curves

Figure 5 shows the three curves we have been discussing as applied to the supergiant E0 galaxy NGC 3379 in the nearby Leo cluster. The data points are from de Vaucouleurs and Capaccioli (1979, Table 2B). The fit of an Oemler template with  $\alpha/\beta = 70$  is shown. The scale unit for this curve is  $B$  mag arcsec $^{-2}$  shown along the left ordinate. The growth curve,  $m_B(r)$ , has the scale on the outer right ordinate. The photometric system is the standard  $B$  band. The  $\eta(r)$  curve has its scale along the inner right ordinate, also in units of magnitudes per square arcseconds. This curve reaches  $\eta(r) = 3$  mag at  $\log r \sim 2.5''$ , or  $r = 316''$ . The  $\eta(r)$  curve is jagged because the *observed*  $B(r_i)$  surface brightness values from de Vaucouleurs and Capaccioli are used in equation (7), and the noise in these values, although small, shows directly as noise in  $\eta(r)$ . This illustrates the high sensitivity of details of the  $\eta(r)$  curve to fluctuations in  $B(r_i)$ . The overall shape of the NGC 3379  $\eta(r)$  curve is well-fitted by an Oemler  $\eta(r)$  template with  $\alpha/\beta = 70$  from the Oemler family in Figure 3a. Note, however, the dip in  $\eta(r)$  in the radius range of  $1.5 < \log r'' < 2.0$  shown well in the  $\eta(r)$  curve, caused by the slight departure of the  $B(r_i)$  data points below the Oemler  $B(r)$  template. This illustrates again how sensitive the shape of  $\eta(r)$  is to even slight variations in the radial intensity profile.

The same point is made again, but stronger, in Figure 6, which shows the calculation of NGC 1272 in the Perseus cluster, based on data obtained by Oemler (1975). He has classified NGC 1272 as a "possible S0." The drawn lines to the  $B(r)$  surface brightness profile (now in the broad-band  $V$  system) is an Oemler template (eq. [2]) with  $\alpha/\beta = 80$ . The deviation of the data from the template for  $\log r'' > 1.2$  is characteristic of galaxies with extended envelopes. Hence, the signature of

extended envelopes in the  $\eta(r)$  curve is the plateau shown in NGC 1272 between  $1.0 < \log r'' < 1.8$ . All supergiants CD galaxies with extended envelopes and all galaxies with disturbed outer envelopes due, for example, to very close companions, exhibit this  $\eta(r)$  plateau.

The final example of a disturbed  $\eta(r)$  curve is for NGC 4267, shown in Figure 7. This galaxy is in the Virgo cluster and is classified as an SB0 galaxy (Sandage and Tammann 1987). The data are from the photometric study of Vigroux *et al.* (1988), which they kindly made available on a readable magnetic tape. The extensive outer envelope, characteristic of S0 and SB0 galaxies, is seen in the deviation of the data points from the adopted Oemler profile template with  $\alpha/\beta = 10$  fitted to the inner data points. The complex  $\eta(r)$  curves magnifies the non-standard run of the  $B(r_i)$  data points, showing that errors in the  $r(\eta)$  radius values for real galaxies are sensitive to the profile. It is important to recall this fact in the next two papers, where scatter in the  $r(\eta)$  radii and in the  $\langle B(r_\eta) \rangle$  average surface brightness are discussed for cluster galaxies in a large sample.

III. RATIO OF  $r(\eta)$  RADII TO THE EFFECTIVE RADII FOR VARIOUS STANDARD TEMPLATES

The observational requirements to make the SB test are set out in the next section, where it will be necessary to know the expected angular diameter at given  $\eta$  values of program galaxies at different redshifts. This necessary scale calibration, in arcseconds, can be made using angular sizes measured for galaxies in the Virgo, Fornax, and Coma Clusters. The data are discussed in detail in the paper that follows (SP), where  $r(\eta)$  and  $r_\eta$  measurements are given for galaxies that have a range of absolute magnitudes. As an aid to relate the size ratios at different  $\eta$  to, say, the Hubble  $a$  value or to  $r_e$ , it is useful to

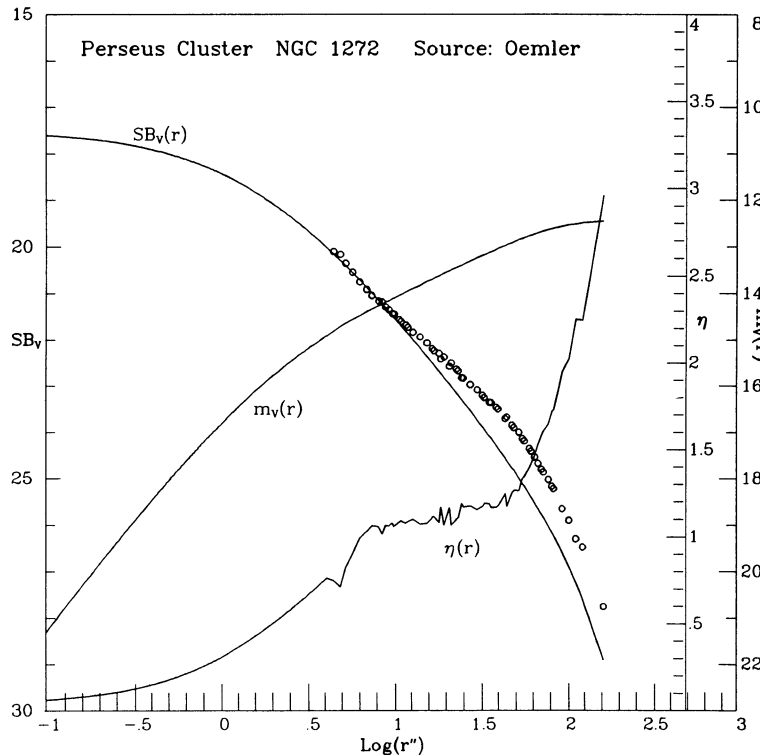


FIG. 6.—Same as Fig. 5 for NGC 1272 in the Perseus cluster. The extended envelope for this S0 galaxy shows as a plateau in the run of  $\eta(r)$ .

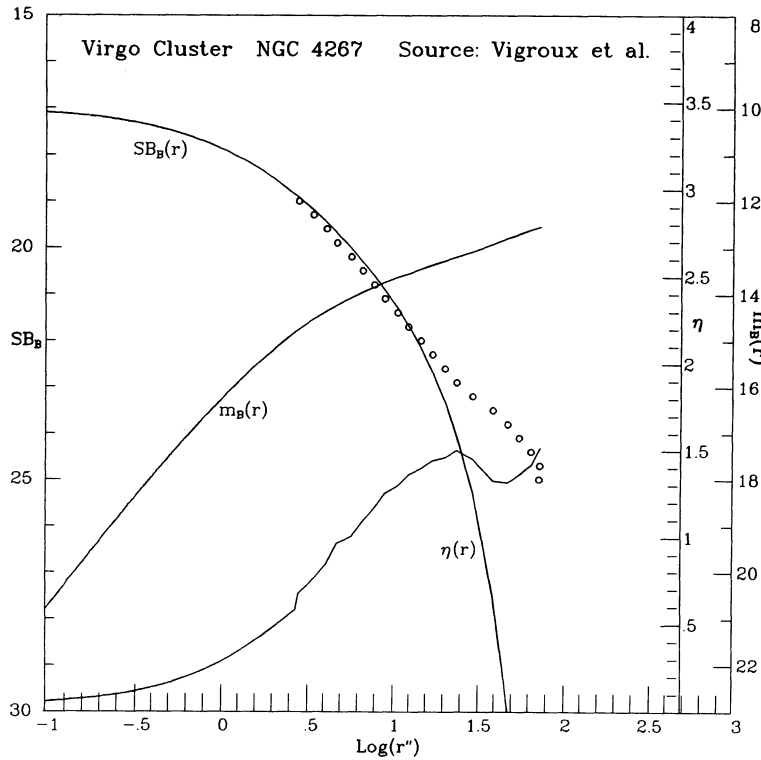


FIG. 7.—Same as Fig. 5 for the SB<sub>0</sub><sub>1</sub> galaxy NGC 4267 on the Virgo Cluster, showing the sensitivity of the shape of the  $\eta(r)$  function to details of the  $B(r)$  surface brightness profile.

calculate the ratios that would be observed if galaxies followed the Hubble, Oemler, or de Vaucouleurs standard templates.

These ratios, found in an obvious way from the numerical integrations used in equations (6) and (7), are listed in Table 1 for  $\eta$  values of 1.0, 1.3, 1.5, 1.7, 2.0, 2.5, 3.0, and 3.5 mag. Column (2) shows the  $r/a$  radii for the Hubble function of equation (1). Columns (3)–(8) give the  $r(\eta)/r_e$  ratios for the Oemler family of equation (2) for  $\alpha/\beta$  values of 100, 60, 30, 20, and 10, and for the de Vaucouleurs template from equation (3). Column (9) shows the slope of the growth curve, in units of  $\text{mag dex}^{-1}$ , corresponding to given  $\eta$  values calculated from equation (5).

Selected values from Table 1 are plotted in Figure 8. The important point is that quite large radii correspond to  $\eta \gtrsim 2$

$\text{mag arcsec}^{-2}$ . These will generally be much larger than the seeing profile, even at redshifts as large as  $z \sim 1$ . However, the intensities are very small at these large radii, and the accuracy that is required to obtain adequate radii measurements for these large  $\eta$  values is high, as shown in the next section.

IV. ASSESSMENT OF THE PARAMETERS OF REAL GALAXIES NEEDED TO APPLY THE SURFACE BRIGHTNESS TEST IN PRACTICE

a) Calibration of the Angular Size Scale from Galaxies in the Virgo Cluster

Figure 9 is a summary of part of the data from the following paper (SP, 1990), showing the correlation of  $r(\eta = 2 \text{ mag})$  and  $r_e$  with apparent  $B$  magnitudes for 56 Virgo Cluster galaxies.

TABLE 1  
RATIOS OF PETROSIAN  $r(\eta)$  RADII TO THE HUBBLE  $a$  RADIUS AND TO THE EFFECTIVE RADIUS FOR THE OEMLER AND DE VAUCOULEURS FITTING FUNCTIONS

$\eta$ (1)	HUBBLE $r/a$ (2)	$r(\eta)/r_e$					Template <sup>a</sup> (8)	$\frac{d \text{ mag}}{d \log r}$ (mag dex <sup>-1</sup> ) (9)
		$\alpha/\beta = 100$ (3)	$\alpha/\beta = 60$ (4)	$\alpha/\beta = 30$ (5)	$\alpha/\beta = 20$ (6)	$\alpha/\beta = 10$ (7)		
1.0.....	4.0	0.38	0.43	0.63	0.78	1.06	0.39	1.99
1.3.....	8.0	0.66	0.86	1.21	1.40	1.63	0.83	1.51
1.5.....	13	1.08	1.35	1.72	1.89	2.11	1.22	1.26
1.7.....	22	1.72	2.02	2.30	2.6	2.39	1.69	1.04
2.0.....	55	3.12	3.22	3.17	3.11	2.89	2.56	0.79
2.5.....	390	5.63	5.08	4.44	4.14	3.61	4.41	0.50
3.0.....	7475	7.70	6.62	5.50	5.00	4.22	6.67	0.32
3.5.....	...	9.42	7.92	6.40	5.75	4.77	9.5	0.20

<sup>a</sup> Ratio for the de Vaucouleurs template from eq. (3).

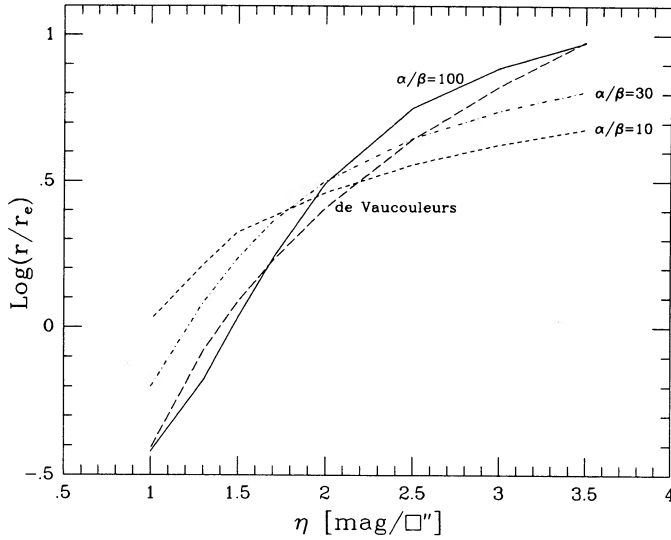


FIG. 8.—The  $r(\eta)/r_e$  ratios for different  $\eta(\text{mag})$  values for the de Vaucouleurs profile and for the three profiles for the Oemler family with  $\alpha/\beta = 100, 30,$  and  $10$  from the data in Table 1.

The left panel shows  $m_B(\eta = 2 \text{ mag})$  magnitudes inside the radius for  $\eta = 2 \text{ mag}$  versus  $\log r$ . The unit for  $r$  is arcseconds. The right panel is similar, showing the correlation using the effective magnitudes and effective radii. Combining Table 1 with the  $r_e$  values in the right panel gives the size expectations for any  $\eta$  value. Lines of constant  $\langle SB \rangle$ , averaged over the  $r(\eta)$  or  $r_e$  radii, are shown, labeled in units of  $B \text{ mag arcsec}^{-2}$ .

The brightest plotted galaxies, reaching  $B(\eta = 2 \text{ mag}) = 10$ , are the supergiant E systems at the top of the Virgo Cluster luminosity function. The first-ranked galaxies of M87 and NGC 4472 are in this sample. There are no brighter galaxies in the cluster.

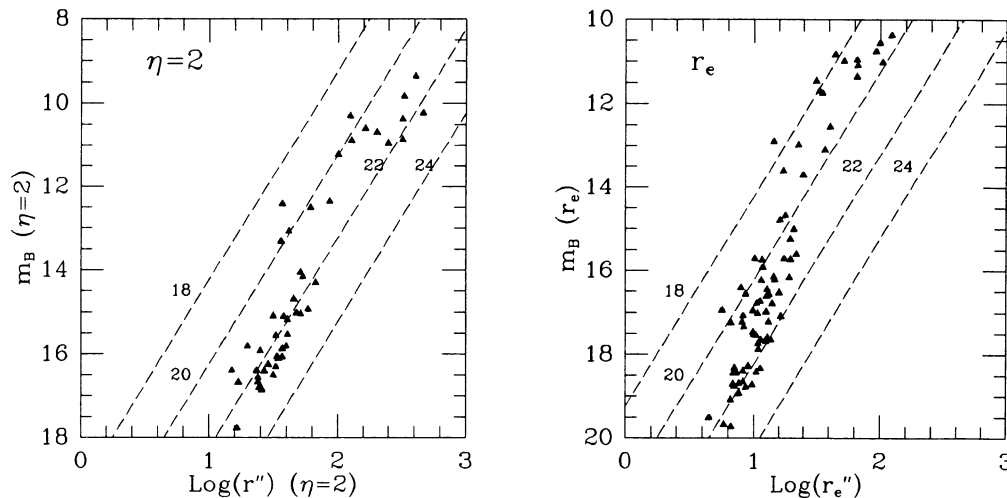


FIG. 9.—Variation of  $\log r(\eta = 2 \text{ mag})$  and of  $\log r_e$  with apparent  $B$  magnitude within the  $\eta = 2 \text{ mag}$  metric radius for 56 galaxies in the Virgo Cluster from data in the following paper (Sandage and Perelmuter 1990). The unit on the abscissa is in arcseconds. Data in this diagram, together with Fig. 8, permit estimates of sizes (in arcseconds) of metric radii to be made of galaxies at different redshifts and absolute magnitudes by appropriate scaling both abscissa and ordinate values for different redshifts relative to Virgo. Lines of constant surface brightness, in  $B \text{ mag arcsec}^{-2}$ , are shown.

These first-ranked members, reaching  $M_{BT} \approx -22.5$ ,  $M_{Be} \approx -21.7$  (using  $m - M = 31.7$  for Virgo Cluster distance modulus), have radii of  $\langle r_e \rangle = 100''$ , and  $\langle r(\eta = 2 \text{ mag}) \rangle = 320''$ . Over the eight magnitudes of the luminosity function sampled by the data in Figure 9, these sizes decrease to  $\langle r_e \rangle \approx 8''$  and  $\langle r(\eta = 2 \text{ mag}) \rangle \approx 15''$  at the Virgo Cluster. To discuss the feasibility of the Tolman test, we now determine the intensity and radius levels of Virgo-like E galaxies placed at various large redshifts.

### b) Parameters of Virgo-like E Galaxies at Larger Redshifts

#### i) Ratio of Radii

In first approximation, the ratio of distances of two clusters at redshifts  $z_1$  and  $z_2$  is  $z_1/z_2$ , and therefore the ratio of angular diameters is  $z_2/z_1$ . For large redshifts, the ratio is more complicated and depends on the space curvature, parameterized by  $q_0$ . These two limiting cases of  $q_0 = \frac{1}{2}$  (i.e.,  $\Omega = 1$ ), and  $q_0 = 0$  are of interest because they undoubtedly bracket the practical case if the standard model applies, and they are particularly simple. We seek the ratio of angular diameters of a “standard galaxy” placed in the Virgo Cluster to those in a distant cluster at redshift  $z$ . We adopt the cosmological redshift of Virgo to be  $z = 0.004$  obtained by adopting the observed redshift to be  $\langle v \rangle = 967 \text{ km s}^{-1}$  and the Local Group infall velocity toward Virgo to be  $220 \text{ km s}^{-1}$  (Sandage and Tammann 1984; Tammann and Sandage 1985, and references therein).

From the standard equations of angular diameter for various redshifts,  $z$ , if the expansion is real, (Sandage 1961a, 1972) we obtain

$$\frac{\theta(\text{distant})}{\theta(\text{Virgo})} = \left( \frac{1+z}{1.004} \right) \frac{(rR_0)_{\text{Virgo}}}{(rR_0)_{\text{distant}}}, \quad (14)$$

where  $rR_0$  is the “interval distance” in the manifold. For the standard model,  $(rR_0)_{\text{Virgo}} = (c/H_0)z_{\text{Virgo}} = 0.004c/H_0$ . For the

$q_0 = \frac{1}{2}$  case of flat spacetime ( $\Omega = 1$ ),

$$rR_0 = \frac{2c}{H_0} \left( 1 - \frac{1}{\sqrt{1+z}} \right). \tag{15}$$

For the  $q_0 = 0$  empty universe case,

$$rR_0 = \left( \frac{c}{H_0} \right) \left( \frac{z}{1+z} \right) \left( 1 + \frac{z}{2} \right) \tag{16}$$

(A standard derivation of eqs. [15] and [16] is in Sandage 1988.) Therefore, for  $q_0 = \frac{1}{2}$ , equations (14) and (15) combine to give

$$\frac{\theta(\text{distant})}{\theta(\text{Virgo})} = \frac{(0.002)(1+z)\sqrt{(1+z)}}{[\sqrt{(1+z)} - 1]}. \tag{17}$$

For  $q_0 = 0$ , the relation is

$$\frac{\theta(\text{distant})}{\theta(\text{Virgo})} = \frac{(0.004)(1+z)}{(z/1+z)[1+(z/2)]}. \tag{18}$$

Equations (17) and (18) give the predictions of how the angular diameters scale with redshift, and therefore how the abscissa values in Figure 9 will decrease as  $z$  increases for V<sub>o</sub>-like galaxies at large distances.

The predictions are listed in Table 2 for various redshifts, based on  $z(\text{Virgo}) = 0.004$ . Columns (2) and (3) show  $rR_0(H_0/c)$  for the  $q_0 = \frac{1}{2}$  and  $q_0 = 0$  geometries. The predicted ratios of angular diameters of identical galaxies to those in Virgo, but at redshift  $z$ , are listed in columns (4) and (5). These ratios decrease more slowly than  $z^{-1}$ , due to the well-known minimum in the predicted  $\theta(z)$  curves for metric diameters for  $q_0 > 0$  at  $z = 1.25$  (Hoyle 1959). In both geometries, the galaxy sizes at  $z \sim 0.7$  are a factor of  $\sim 0.01$  of those at Virgo.

From Figure 9, the largest galaxies have  $r(\eta = 2) \sim 300''$ , or diameters of  $600''$ . Hence, similar galaxies at  $z \sim 0.7$  are expected to have diameters at  $\eta = 2$  of  $6''$ , large enough to be easily measured and appropriately corrected with high precision for the seeing profile, whose characteristic size will be small compared with such source diameters. If we can measure galaxies with  $r(2 \text{ mag})$  diameters of  $1''$ , again with a convolution correction for seeing, we can sample about 4 mag into the luminosity function at  $z = 0.7$ , on the assumption that  $m \sim 5 \log r$  approximately, which is, of course, the constant surface brightness condition that is correct in the lowest approximation (Hubble 1926). The relatively small deviations from

the constant surface brightness condition is the subject of the two papers that follow (SP, 1990).

ii) *Ratio of Apparent Magnitudes and Surface Brightnesses to Virgo*

Although the angular sizes of the galaxies within the first 4 mag of the luminosity function are large enough to be well above the seeing profile, and therefore can be well corrected for seeing smearing, we inquire now into the expected apparent luminosity levels. With the diameter ratios in columns (4) and (5) in Table 2, and with the assumption that the surface brightness decreases as  $(1+z)^n$  with redshift, we calculate in an obvious way the apparent magnitude difference between a standard galaxy in Virgo and in a distant cluster at redshift  $z$ . Consider the case of  $z = 0.7$  in a  $q_0 = 0$  geometry. The ratio of the galaxian areas between Virgo and the distant clusters is the square of the column (5) diameter ratio. For  $z = 0.7$ , this area ratio is  $5 \log$  (diameter ratio), which is 9.6 mag. If the bolometric SB has decreased by  $(1+z)^4$  due to the expansion, the bolometric magnitude difference between Virgo and the cluster standard galaxy is then  $9.6 + 2.3 \text{ mag} = 11.9 \text{ mag}$ ; (see col. [6] of Table 2 for  $z = 0.7$ ).

However, in using a detector of finite bandwidth rather than a bolometer, there is an additional decrease in SB by  $2.5 \log(1+z)$  mag due to the stretching of the redshifted spectrum by the factor of  $1+z$  relative to the detector bandwidth. This gives a total correction of  $(1+z)^5$  to the SB, assuming a flat intrinsic spectrum (in intensity per unit wavelength interval) (i.e., if the selective  $K$  term were zero [see Humason, Mayall, and Sandage 1956, Appendix B; Oke and Sandage 1968 for a discussion of the separate selective and bandwidth terms in the total  $K$  correction]). If the spectrum is not flat (again per unit wavelength interval), an additional dimming by the selective part of the  $K$  correction must also be applied. For the moment, we assume the selective part to be zero (i.e., we suppose that the observations are to be made in the  $I$  band, where this is almost true; a more accurate example with more detail is set out in Paper III). The  $(1+z)^5$  dimming ratios are listed in column (7) of Table 2.

According to Table 2, the standard galaxies will be  $9.6 + 2.88 = 12.5 \text{ mag}$  fainter for  $z = 0.7$  than in Virgo if  $K(\text{selective}) = 0$ . Because  $B - R \simeq 2 \text{ mag}$  for  $E$  galaxies in Virgo (Sandage 1973a, Fig. 4), the ordinate in Figure 9 shows that  $R \simeq 8 \text{ mag}$  in the  $R$  bandpass for the brightest Virgo galaxies. Direct measurement (Sandage 1973b, Tables 1 and 4) has given  $R(\text{total}) = 7.6 \text{ mag}$  for the first-ranked Virgo cluster galaxy. Hence, at  $z = 0.7$ , the observed magnitude to the

TABLE 2  
PREDICTED ANGULAR DIAMETER RATIOS RELATIVE TO GALAXIES IN THE VIRGO CLUSTER

z	$rR_0$		$\theta_d/\theta_v$		EXPANSION		NO EXPANSION	
	$2 \left[ 1 - \left( \frac{1}{\sqrt{1+z}} \right) \right]$	$\left( \frac{z}{1+z} \right) \left[ 1 + \left( \frac{z}{2} \right) \right]$	$(q_0 = \frac{1}{2})$	$(q_0 = 0)$	$(1+z)^4$	$(1+z)^5$	$(1+z)$	$(1+z)^2$
	$(q_0 = \frac{1}{2})$	$(q_0 = 0)$	(4)	(5)	(mag)	(mag)	(mag)	(mag)
(1)	(2)	(3)	(4)	(5)	(6)	(7)	(8)	(9)
0.1.....	0.0931	0.0954	0.047	0.046	0.41	0.52	0.10	0.21
0.3.....	0.2459	0.2654	0.021	0.020	1.14	1.42	0.28	0.57
0.5.....	0.3670	0.3833	0.016	0.016	1.76	2.20	0.44	0.88
0.7.....	0.4661	0.5559	0.015	0.012	2.30	2.88	0.58	1.15
1.0.....	0.5858	0.7500	0.014	0.011	3.01	3.76	0.75	1.50
1.5.....	0.7351	1.0500	0.014	0.010	3.98	4.97	0.99	1.99
2.0.....	0.8453	1.3333	0.014	0.009	4.77	5.96	1.19	2.38

$r(\eta = 2 \text{ mag})$  radius should be approximately  $7.5 + 12.5 = 20$  mag in  $R$ . Because we are assuming that  $\eta = 2 \text{ mag arcsec}^{-2}$  at our measuring point along the profile, the SB at  $r(\eta = 2 \text{ mag})$  will be  $20 + 2 = 22$  mag in  $R$ . The angular sizes are still large enough to be able to be corrected accurately for the seeing profile for galaxies as much as  $\sim 4$  mag into the luminosity function, giving  $R = 24$  over the area to  $\eta = 2 \text{ mag}$ , and  $B(r) = 26 R$  mag at this radius.

These magnitude levels are well brighter than the limit to which observations can be made with existing telescopes. Hence, because (1) the necessary angular resolution can be attained, and (2) the flux levels to be measured (for, at least, first-ranked and somewhat fainter galaxies) are well within technical capabilities, the Tolman SB test is at least feasible, providing that the  $\langle B(\eta) \rangle$  values from galaxy to galaxy are stable enough, as discussed in a paper that follows.

### iii) Expected Luminosity Evolution in the Look-Back Time

The one remaining possible stumbling block concerning the feasibility of performing the test is whether the expected luminosity evolution in the look-back time is larger than the expansion effect or not. For passive evolution (i.e., simple burning down of the main-sequence termination point in the HR diagram with time), we show now that the expected luminosity change is, in fact, smaller than the  $(1+z)^4$  effect we seek.

An early estimate (Sandage 1961*b*) based on passive evolution and a flat main-sequence luminosity function for the aggregate luminosity, gave a luminosity brightening with look-back time of  $\sim 0.10 \text{ mag } 10^{-9} \text{ yr}$ . This was an overestimate by  $\sim 30\%$ , because the main-sequence luminosity function is not flat. Elaborate calculations by Tinsley (1968, 1972*a*, *b*, 1976,

1980, and references therein) did show that the expected luminosity brightening due to passive evolution is in fact,  $\sim 30\%$  smaller than this first estimate. Tinsley's evolutionary brightening can be well approximated by  $\Delta \text{ mag}(z) = 2.5 \log(1+z)$ .

This expected passive evolutionary brightening is, then, much smaller than the Tolman  $(1+z)^4$  dimming factor, showing that the correction for evolution, although important and necessary, is not expected to overwhelm the  $(1+z)^4$  effect in the Tolman test. Of much more critical concern is if the concept of "standard galaxies" at different distances can be invoked. To this end, we inquire in the papers that follow as to (1) how small the dispersion in  $\langle B(\eta) \rangle$  at a given absolute magnitude is for different  $\eta$  values, and (2) how large the systematic variation of  $\langle B(\eta) \rangle$  with absolute magnitude for E galaxies is in the nearby Virgo, Fornax, and Coma Clusters, and in the local field.

We wish to thank Augustus Oemler, Patricia Vader and L. Vigroux, and James Schombert for sending their detailed intensity profile measurements for a number of galaxies studied here. Their large data bases have been used extensively in the later papers of this series, to be published, but selected samples of the data have also been used in the present paper. We also wish to thank Vahe Petrosian for reading and commenting on an early draft. The suggestion of the unknown referee to emphasize the difficult problems which various evolutionary effects might have at large redshifts is appreciated, and has been put in some detail in § I. As so often before, it is again a pleasure to thank Janet Krupsaw of The Johns Hopkins University, Department of Physics and Astronomy for her careful preparation of the many drafts of this paper.

### REFERENCES

- Baum, W. A. 1972, in *IAU Symposium 44, External Galaxies and Quasi-stellar Objects*, ed. D. S. Evans (Dordrecht: Reidel), p. 393.  
 Bingelli, B., Sandage, A., and Tarenghi, M. 1984, *A.J.*, **89**, 64.  
 de Vaucouleurs, G. 1958, in *Handbuch der Physik*, Vol. 53, ed. S. Flugge (Berlin: Springer), p. 311.  
 ———. 1962, in *IAU Symposium 15, Problems of Extragalactic Research*, ed. G. McVittie (New York: Mcmillan), p. 3.  
 de Vaucouleurs, G., and Capaccioli, M. 1979, *Ap. J. Suppl.*, **40**, 699.  
 Djorgovski, S. B. 1985, Ph.D. thesis, University of California at Berkeley.  
 Djorgovski, S. B., and Spinrad, H. 1981, *Ap. J.*, **251**, 417.  
 Geller, M. J., and Peebles, P. J. E. 1972, *Ap. J.*, **174**, 1.  
 Hoyle, F. 1959, in *IAU Symposium 9, Radio Astronomy*, ed. R. N. Bracewell (Stanford: Stanford University Press), p. 529.  
 Hubble, E. 1926, *Ap. J.*, **64**, 321.  
 ———. 1930, *Ap. J.*, **71**, 231.  
 Hubble, E., and Tolman, R. C. 1935, *Ap. J.*, **82**, 302.  
 Humason, M. L., Mayall, N. U., and Sandage, A. 1956, *A.J.*, **61**, 97.  
 Jedrzejewski, R. I. 1987, *M.N.R.A.S.*, **226**, 747.  
 Jedrzejewski, R. I., Davies, R. L., and Illingworth, G. D. 1988, *A.J.*, **94**, 1508.  
 King, I. R. 1966, *A.J.*, **71**, 64.  
 ———. 1978, *Ap. J.*, **222**, 1.  
 Oemler, A. 1975, Ph.D. thesis, California Institute of Technology.  
 ———. 1976, *Ap. J.*, **209**, 693.  
 Oke, J. B., and Sandage, A. 1968, *Ap. J.*, **154**, 21.  
 Petrosian, V. 1976, *Ap. J. (Letters)*, **209**, L1.  
 Sandage, A. 1961*a*, *Ap. J.*, **133**, 355.  
 ———. 1961*b*, *Ap. J.*, **134**, 916.  
 ———. 1972, *Ap. J.*, **173**, 485.  
 ———. 1973*a*, *Ap. J.*, **183**, 711.  
 ———. 1973*b*, *Ap. J.*, **183**, 731.  
 ———. 1988, *Ann. Rev. Astr. Ap.*, **26**, 561.  
 Sandage, A., and Perelmuter, J. M. 1990, *Ap. J.*, submitted.  
 Sandage, A., and Tammann, G. A. 1984, in *ESO-CERN Symposium 1, Large Scale Structure of the Universe, Cosmology, and Fundamental Physics*, ed. G. Setti and L. Van Hove (Geneva: CERN), p. 127.  
 ———. 1987, *A Revised Shapley-Ames Catalog of Bright Galaxies*, Carnegie Institution of Washington Publication 635 (2d ed.).  
 Tammann, G. A., and Sandage, A. 1985, *Ap. J.*, **294**, 81.  
 Tinsley, B. M. 1968, *A.J.*, **151**, 547.  
 ———. 1972*a*, *Ap. J. (Letters)*, **173**, L93.  
 ———. 1972*b*, *Astr. Ap.*, **20**, 383.  
 ———. 1976, *Ap. J.*, **203**, 63.  
 ———. 1980, *Ap. J.*, **241**, 41.  
 Tolman, R. C. 1930, *Proc. Nat. Acad. Sci.*, **16**, 511.  
 ———. 1934, *Relativity Thermodynamics and Cosmology*. Oxford: Oxford University Press).  
 Vigroux, L., Souviron, J., Lachieze-Rey, M., and Vader, J. P. 1988, *Astr. Ap. Suppl.*, **73**, 1.

JEAN-MARC PERELMUTER: Department of Physics and Astronomy, The Johns Hopkins University, Homewood Campus, Baltimore, MD 21218

ALLAN SANDAGE: The Observatories of the Carnegie Institution of Washington, 813 Santa Barbara Street, Pasadena, CA 91101-1292